Journal of Alloys and Compounds 503 (2010) 233–236

Contents lists available at ScienceDirect

Journal of Alloys and Compounds

journal homepage: www.elsevier.com/locate/jallcom

Composition and film thickness effects on microstructure and magnetic properties of ordered $L1_0$-structured $Fe_{100-x}Pt_x$ films

W.B. Mi [a,*], J.J. Shen [b], W.J. Lu [a], H.L. Bai [a]

[a] Tianjin Key laboratory of Low Dimensional Materials Physics and Preparing Technology, Institute of Advanced Materials Physics, Faculty of Science, Tianjin University, Tianjin 300072, People's Republic of China
[b] Department of Mathematics and Physics, Shijiazhuang Railway Institute, Shijiazhuang 050043, People's Republic of China

ARTICLE INFO

Article history:
Received 24 March 2010
Received in revised form 25 April 2010
Accepted 29 April 2010
Available online 6 May 2010

PACS:
75.75.+a
75.70.Ak
75.70.−i
75.50.−y

Keywords:
$L1_0$ phase
FePt
Magnetocrystalline anisotropy
Magnetic properties

ABSTRACT

$Fe_{100-x}Pt_x$ films with different Pt atomic fractions (x) and film thicknesses (t_f) were fabricated by magnetron sputtering at room temperature and subsequently annealed at 650 °C. Their structure and magnetic properties have been investigated systematically. All the as-deposited $Fe_{100-x}Pt_x$ films with disordered face-centered-cubic (fcc) structure are soft ferromagnetic. The annealed $Fe_{100-x}Pt_x$ films evolve from Fe_3Pt, FePt to $FePt_3$ with increasing x. High-temperature annealing makes the $Fe_{100-x}Pt_x$ films transform from the disordered fcc structure to the ordered face-centered-tetragonal (fct) $L1_0$ structure as x is in the range of 40–60. The grain size of the annealed $Fe_{52}Pt_{48}$ films increases with increasing t_f. All the annealed $Fe_{100-x}Pt_x$ films are hard ferromagnetic. The coercivity of the annealed $Fe_{100-x}Pt_x$ films first increases, and decreases latterly with increasing x. Meanwhile, the coercivity of the annealed $Fe_{52}Pt_{48}$ films decreases with increasing temperature.

1. Introduction

In recent years, great improvements have been made on high-density perpendicular magnetic recording media. The magnetic recording density has increase rapidly in laboratory research [1]. For high-density magnetic recording media, thermal stability is becoming a serious obstacle for the practical applications due to the decrease of the recording unit size. Intensive studies for overcoming the above problem have been carried out on the ordered face-centered-tetragonal (fct) $L1_0$-FePt alloy with a large magnetocrystalline anisotropy constant K_u of $\sim 7 \times 10^7$ erg/cm^3. The large K_u can result in a coercivity as large as 120 kOe theoretically by assuming that there are no other anisotropies. The FePt films fabricated by the magnetron sputtering without substrate heating generally have a disordered face-centered-cubic (fcc) structure. High-temperature annealing above 500 °C is necessary for the FePt films to transform from the disordered fcc structure into the ordered fct structure [2,3], and above 650 °C for the FePt based nanocomposite films [4–8]. The third element doped into the FePt films makes the transformation temperature decrease because of the increase of the diffusivities of Fe and Pt atoms [9,10]. Furthermore, top layers or sublayers including Ag, Pt and GePt can also affect the microstructure and magnetic properties of the FePt layers [11–14]. It is well known that the composition and film thickness of the nanoscale films affects the structure and properties of the films intensively. Yu et al. reports that the magnetic properties of the annealed FePt nanoparticles fabricated using a solution-phase method can be affected by the Pt concentration [15]. Toney et al. found that the structure and magnetic properties of the FePt films with film thickness less than 10 nm are related to the film thickness [16]. Shima et al. study the variation of the morphology and magnetic properties of the FePt films on MgO substrates with different film thicknesses less than 100 nm [17]. However, the effect of the composition and film thickness on the structure and magnetic properties of the FePt films with wide range of composition and film thickness is still not clear. In this paper, the $Fe_{100-x}Pt_x$ films with different Pt atomic fractions (x) and film thicknesses (t_f) were fabricated using the magnetron sputtering at room temperature and subsequently annealed at 650 °C for one hour in a 10^{-6} Pa vacuum. Structure and magnetic properties of

* Corresponding author.
E-mail address: miwenbo@tju.edu.cn (W.B. Mi).

0925-8388/$ – see front matter © 2010 Elsevier B.V. All rights reserved.
doi:10.1016/j.jallcom.2010.04.245

the as-deposited and annealed $Fe_{100-x}Pt_x$ films were investigated systematically.

2. Experimental details

$Fe_{100-x}Pt_x$ films with different Pt atomic fractions (x) and film thicknesses (t_f) were deposited on Si (1 0 0) wafers using a DC magnetron sputtering system at room temperature. When the base pressure of the chamber reaches 8.0×10^{-6} Pa or better, Ar (99.999%) gas was introduced into the chamber till 0.5 Pa. Then the sputtering was carried out from pure Fe (99.999%) targets on which pure Pt (99.99%) pieces were placed. The film thicknesses were determined using a Dektak 6M surface profiler. The as-deposited $Fe_{100-x}Pt_x$ films fabricated on Si (1 0 0) wafers were subsequently annealed at 650 °C for one hour in a 10^{-6} Pa vacuum. X-ray photoelectron spectroscopy (XPS) and X-ray diffractometer (XRD) were used to measure the composition, chemical state and structure of the samples. The X-ray photoelectron (XPS) spectra were recorded in a PHI5600 spectrometer equipped with a spherical capacitor analyzer, using Mg Kα radiation (1253.6 eV) with a resolution of 0.25 eV. The background pressure in the analysis chamber was maintained at 2.2×10^{-10} Torr, and the operating pressure was less than 1.5×10^{-9} Torr. For removing the contaminated surface layer, Ar ions with 2-keV energy, a current density of 1 mA/mm^2 and an incidence angle of 45° were used to sputter the film surface. The magnetic properties were measured using a vibrating sample magnetometer (VSM, LDJ9600-1) at room temperature and Quantum Design physical property measurement system (PPMS-9) at temperatures from 5 to 305 K.

3. Results and discussion

3.1. Microstructure

XPS measurements taken at $h\nu = 1253.6$ eV were performed with an emphasis on the peaks associated with Fe_{2p}, Pt_{4f}, C_{1s} and O_{1s} for analyzing the atomic fractions and chemical states of each element in the samples. The C_{1s} and O_{1s} peaks disappear after 1.5-min Ar^+ ion bombardment (2 keV) on the film surface, implying that the contaminated C and O on the film surface have been removed. Fig. 1 shows the typical XPS patterns of the 120-nm thick $Fe_{100-x}Pt_x$ films. Due to spin–orbit coupling, the Fe_{2p} core levels split into $2p_{1/2}$ and $2p_{3/2}$ components. In Fig. 1(a), the Fe $2p_{1/2}$ and $2p_{3/2}$ components situate at 707.7 and 720.7 eV, which are from Fe^0. In Fig. 1(b), the peaks of Pt_{4f} locate at 72.8 and 76.3 eV, which are from Pt^0. The XPS

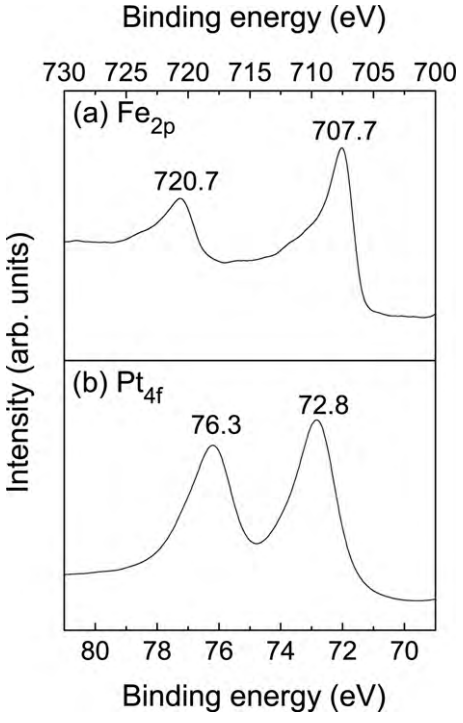

Fig. 1. Typical XPS patterns of the 120-nm thick $Fe_{100-x}Pt_x$ films, (a) Fe_{2p} and (b) Pt_{4f}.

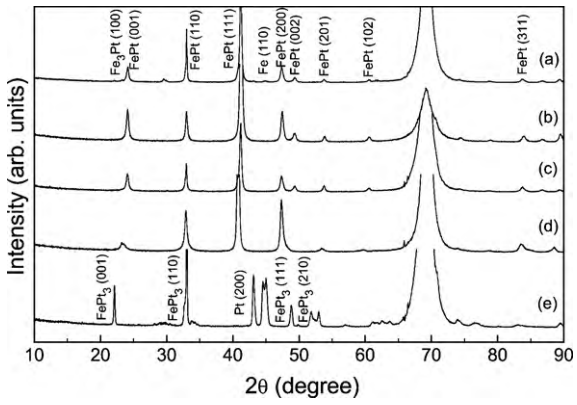

Fig. 2. XRD patterns of the 650 °C annealed 120-nm thick $Fe_{100-x}Pt_x$ films with different x, (a) $x = 30$, (b) $x = 43$, (c) $x = 48$, (d) $x = 56$ and (e) $x = 64$.

results of the $Fe_{100-x}Pt_x$ films reveal that the films are composed of metallic Fe and Pt.

Fig. 2 shows the XRD patterns of the 650 °C annealed 120-nm thick $Fe_{100-x}Pt_x$ films with different x. In Fig. 2(a), the diffraction peaks from Fe (1 1 0) and Fe_3Pt (1 0 0) can be observed, revealing that there are Fe and Fe_3Pt in the films. In Fig. 2(b)–(d), the diffraction peaks from the ordered fct FePt (0 0 1), (1 1 0), (1 1 1), (2 0 0), (0 0 2), (2 0 1), (1 0 2) and (3 1 1) appear, which can be explained by the facts that the ordered fct structure of FePt alloy can be formed as x is in the range of 40–60. However, the diffraction peaks in Fig. 2(d) shift to the low angles, suggesting that the lattice constants become larger. In Fig. 2(e), the diffraction peaks of the film with $x = 64$ are from $FePt_3$ (0 0 1), (1 1 0), (1 1 1), (210), Fe (1 1 0) and Pt (2 0 0). The XRD results confirm that the main phases in the annealed $Fe_{100-x}Pt_x$ films transform from Fe_3Pt, FePt to $FePt_3$ as x increases from 30 to 64.

Fig. 3 displays the XRD patterns of the 650 °C annealed $Fe_{52}Pt_{48}$ films with different t_f. In Fig. 3, the diffraction peaks of all the annealed $Fe_{52}Pt_{48}$ films with different t_f are from ordered fct FePt (0 0 1), (1 1 0), (1 1 1), (2 0 0), (0 0 2), (2 0 1), (1 0 2) and (3 1 1) lattices, which suggest that all the films have ordered fct structure. The calculated lattice constants based on Bragg's law from Fig. 3 are $a = b = 0.383$ nm and $c = 0.369$ nm for the 120-nm thick $Fe_{52}Pt_{48}$ films, and $a = b = 0.382$ nm and $c = 0.367$ nm for 30, 60, and 90-nm thick $Fe_{52}Pt_{48}$ films respectively. The lattice constants are a little smaller than that (0.384 nm and 0.371 nm) of the bulk FePt single crystal sample. The reduction of the lattice constants may be due to the coordination number (CN) imperfection induced bond contraction of atoms in the surface/interface region [18]. The grain size was estimated by Scherrer's formula using the width of the (1 1 1)

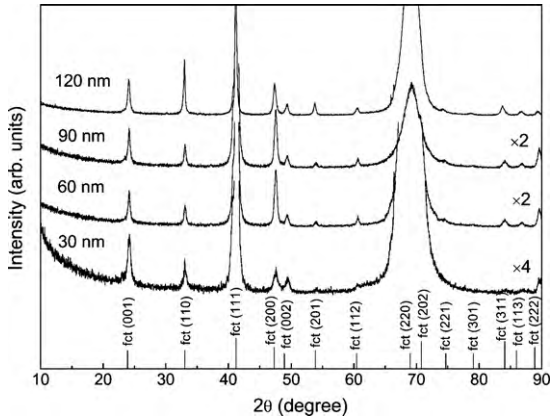

Fig. 3. XRD patterns of the 650 °C annealed $Fe_{52}Pt_{48}$ films with different t_f.

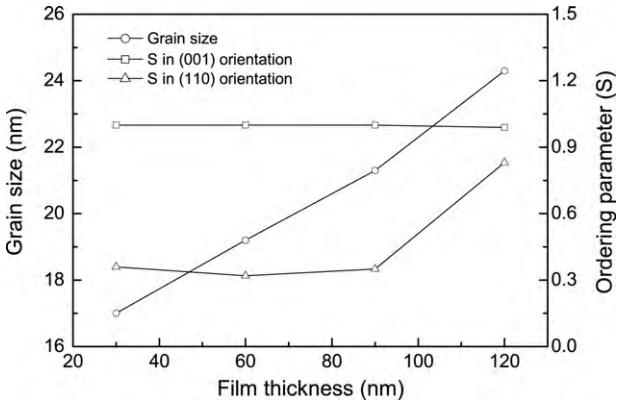

Fig. 4. Dependence of grain size and ordering parameter (S) of the 650 °C annealed $Fe_{52}Pt_{48}$ films on t_f.

peak from the XRD spectra, as following [19]

$$D = \frac{0.89\lambda}{B\cos(\theta)}, \quad (1)$$

where λ is the X-ray wavelength, θ the diffraction angle, and B is the full peak width at half-height. From Fig. 4, one can see that the average grain size increases from ~17 nm at t_f = 30 nm to ~24 nm t_f = 120 nm.

Due to the dependence of the magnetocrystalline anisotropy on the ordering degree of Fe and Pt atoms in the ordered fct structure significantly, it is necessary to investigate the ordering degree of the ordered fct FePt. The chemical ordering degree of the FePt alloy can be obtained by determining the one-dimensional chemical ordering parameter S defined as [20–23]

$$S = \frac{r_{Fe} - x_{Fe}}{y_{Pt}} = \frac{r_{Pt} - x_{Pt}}{y_{Fe}}, \quad (2)$$

where $r_{Fe(Pt)}$ is the fraction of Fe(Pt) sites occupied by the correct atomic species, $x_{Fe(Pt)}$ is the atomic fraction of Fe(Pt) in the sample (1/2 for equiatomic stoichiometry), and $y_{Fe(Pt)}$ is the fraction of Fe(Pt) sites (1/2 for equiatomic stoichiometry). The fraction (w_{Fe}) of Fe sites occupied by Pt atoms is

$$w_{Fe} = 1 - r_{Fe}, \quad (3)$$

and for a perfectly ordered FePt crystal S = 1 and r_{Fe} = 1. A perfectly disordered crystal has S = 0, r_{Fe} = 1/2, and w_{Fe} = 1/2.

Experimentally, S is defined by the following equation [23],

$$S^2 = \frac{[I_{(1\,1\,0)}/I_{(1\,1\,1)}]_{experiment}}{[I_{(1\,1\,0)}/I_{(1\,1\,1)}]_{calculated}} \quad (4)$$

or

$$S^2 = \frac{[I_{(0\,0\,1)}/I_{(0\,0\,2)}]_{experiment}}{[I_{(0\,0\,1)}/I_{(0\,0\,2)}]_{caculated}} \quad (5)$$

where $I_{(h\,k\,l)}$ is the intensity of the ($h\,k\,l$) diffraction peak. In Fig. 4, the ordering parameter S calculated using Eq. (4) increases with increasing t_f. However, the value calculated using Eq. (5) is almost near 100% at t_f ranging from 30 to 90 nm. At t_f = 120 nm, the ordering parameter S is 98.9%. The calculated results indicate that the decrease of the film thickness improves the film growth along the (0 0 1) orientation because the lattice constant c is smaller than a and b, and does not improve the ordering degree along the (1 1 0) orientation. From the above analyses, the total ordering degree in different orientations of the annealed $Fe_{52}Pt_{48}$ films is improved by increasing the film thickness.

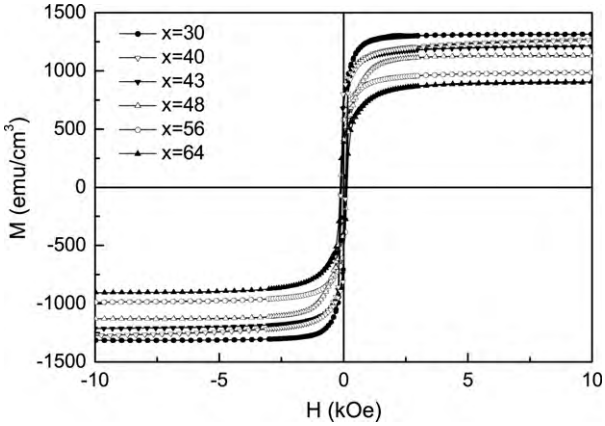

Fig. 5. Room-temperature M–H curves of the as-deposited 120-nm thick $Fe_{100-x}Pt_x$ films with different x.

3.2. Magnetic properties

Fig. 5 displays the room-temperature M–H curves of the as-deposited 120-nm thick $Fe_{100-x}Pt_x$ films with different x. It is clear from this figure that all the as-deposited $Fe_{100-x}Pt_x$ films are soft ferromagnetic because the as-deposited films are disordered fcc structure with small magnetocrystalline anisotropy. It is well known that the film deposition by sputtering is not a equilibrium process and the substrate temperature is too low for Fe and Pt atoms to form the ordered $L1_0$ structure with large magnetocrystalline anisotropy. The saturation magnetization of the as-deposited $Fe_{100-x}Pt_x$ films decreases from 1300 to 880 emu/cm^3 when x increases from 30 to 64 due to the decrease of the Fe atomic fraction.

Fig. 6 presents the room-temperature M–H curves of the 650 °C annealed 120-nm thick $Fe_{100-x}Pt_x$ films with different x. From this figure, it is clear that all the $Fe_{100-x}Pt_x$ films are hard ferromagnetic. Some hysteresis loops of the annealed films exhibit a two-step saturation behavior. The rapidly saturated part is from soft ferromagnetic phase, and the slowly saturated part from the hard ferromagnetic ordered fct phase. For the films with x = 43, 48 and 56, the soft saturation part should be from the surface oxides due to the exposure in air and/or the soft ferromagnetic phases in the films even though the oxide phase can not be detected by XRD. In the present manuscript, the coercivity was obtained by using the relation of $H_c = \left|H_{c+} - H_{c-}\right|/2$, where H_{c+} and H_{c-} are the crossover points of the M–H curves and H axis. Obviously, the relatively high

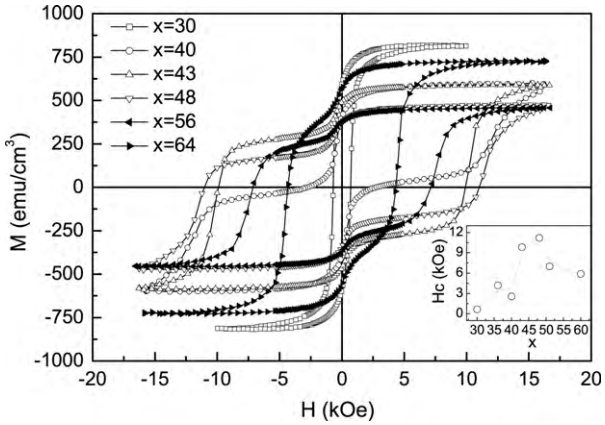

Fig. 6. Room-temperature M–H curves of the 650 °C annealed 120-nm thick $Fe_{100-x}Pt_x$ films with different x. The inset gives the dependence of the coercivity of the annealed $Fe_{100-x}Pt_x$ films on x.

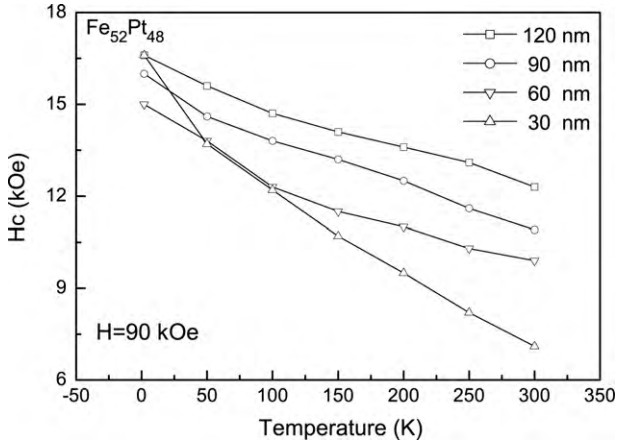

Fig. 7. Temperature dependence of the in-plane coercivity of the 650 °C annealed $Fe_{52}Pt_{48}$ films with different t_f.

coercivity (~12 kOe) arises from the ordered fct phase with high magnetocrystalline anisotropy. As x is lower than 48, the coercivity of the annealed films increases with increasing x because the volume fraction of the ordered fct phase increases. At $x > 48$, the coercivity of the annealed films decreases because the ordered fct structure was destroyed or the films are mainly composed of antiferromagnetic $FePt_3$ with a Neel temperature of 160 K. At $x = 56$, the lattice constant increases, which can decrease the magnetocrystalline anisotropy of the films, so that the coercivity decreases. At $x = 64$, soft ferromagnetic Fe should exist in the films because the diffraction from bcc Fe (1 1 0) can be observed in the XRD patterns as shown in Fig. 2. Meanwhile, some diffraction peaks from the fct phase can also be observed, so that the films are not paramagnetic at room temperature.

The as-deposited $Fe_{52}Pt_{48}$ films with different t_f are soft ferromagnetic because the substrate temperature is too low for Fe and Pt atoms to form the ordered fct structure with large magnetocrystalline anisotropy. Meanwhile, the saturation magnetization almost keeps at a constant of 1140 emu/cm^3 as t_f changes. In order to improve the atomic mobility to the correct position of the ordered fct lattice, the as-deposited films were annealed at 650 °C. After being annealed at 650 °C for one hour, the $Fe_{52}Pt_{48}$ films are ferromagnetic. The room-temperature coercivity of the annealed $Fe_{52}Pt_{48}$ films increases as t_f increases. Fig. 7 shows the temperature dependence of the coercivity of the 650 °C annealed $Fe_{52}Pt_{48}$ films with different t_f. From Fig. 7, it is clear that the coercivity of the films with $t_f = 90$ and 120 nm decreases linearly with increasing temperature, suggesting that the magnetization mechanism is dominant by domain wall motion with strong magnetic interactions. However, the coercivity of the films with $t_f = 60$ and 30 nm decrease rapidly and approach $T^{1/2}$ relation, which reveals that there are some small particles those follow Stoner–Wohlfarth rotation model, which may be ascribed to the decrease of the grain size as the film thickness decreases.

4. Conclusions

Structure and magnetic properties of the $Fe_{100-x}Pt_x$ films with different x and t_f fabricated by sputtering were studied systematically. All the as-deposited $Fe_{100-x}Pt_x$ films are soft ferromagnetic. High-temperature annealing makes the $Fe_{100-x}Pt_x$ films transform from the disordered fcc structure into the ordered fct structure. The grain size of the $Fe_{52}Pt_{48}$ films increases with increasing t_f. Meanwhile, the annealed $Fe_{100-x}Pt_x$ films are hard ferromagnetic due to the improvement of the chemical ordering degree and the coercivity increases with t_f measured at room temperature, and decreases with the increase of the measuring temperature.

Acknowledgements

This work was supported by NSFC of China (50701033), the RFDP (20070056047), TSTC (08JCYBJC09400) and Young Faculty Foundation of Tianjin University (TJU-YFF-08B52 and 08A05).

References

[1] D. Weller, A. Moser, L. Folks, M.E. Best, W. Lee, M.F. Toney, M. Schwickert, J.U. Thiele, M.F. Doerner, IEEE Trans. Magn. 36 (2000) 10.
[2] R.A. Ristau, K. Barmak, L.H. Lewis, K.R. Coffy, J.K. Howard, J. Appl. Phys. 86 (1999) 4527.
[3] C.M. Kuo, P.C. Kuo, H.C. Wu, J. Appl. Phys. 85 (1999) 2264.
[4] M. Watanabe, T. Masumoto, D.H. Phing, K. Hono, Appl. Phys. Lett. 76 (2000) 3971.
[5] S.C. Chen, P.C. Kuo, C.T. Lie, J.T. Hua, J. Magn. Magn. Mater. 236 (2001) 151.
[6] S.C. Chen, P.C. Kuo, A.C. Sun, C.T. Lie, W.C. Hsu, Mater. Sci. Eng. B 88 (2002) 91.
[7] C.P. Luo, D.J. Sellmyer, Appl. Phys. Lett. 75 (1999) 3162.
[8] R.J. Tang, W.L. Zhang, Y.R. Li, J. Alloys Compd. 496 (2010) 380.
[9] Y.K. Takahashi, M. Ohnuma, K. Hono, J. Magn. Magn. Mater. 246 (2002) 259.
[10] M. Tomoyuki, K. Tadashi, K. Akila, N. Toshihiko, J. Akiyama, Appl. Phys. Lett. 80 (2002) 2147.
[11] K.F. Dong, X.F. Yang, J.B. Yan, W.M. Cheng, X.M. Cheng, X.S. Miao, X.H. Xu, F. Wang, J. Alloys Compd. 476 (2009) 662.
[12] J.L. Tsai, G.B. Lin, H.T. Tzeng, J. Alloys Compd. 487 (2009) 18.
[13] C.W. Hsu, S.K. Chen, W.M. Liao, F.T. Yuan, W.C. Chang, J.L. Tsai, J. Alloys Compd. 449 (2008) 52.
[14] J.L. Tsai, C.J. Hsu, J. Alloys Compd. 455 (2008) 87.
[15] A.C.C. Yu, M. Mizuno, Y. Sasaki, H. Kondo, Appl. Phys. Lett. 85 (2004) 6242.
[16] M.F. Toney, W.Y. Lee, J.A. Hedstrom, A. Kellock, J. Appl. Phys. 93 (2003) 9902.
[17] T. Shima, K. Takanashi, Y.K. Takahashi, K. Hono, Appl. Phys. Lett. 85 (2004) 1050.
[18] C.Q. Sun, S. Li, B.K. Tay, Appl. Phys. Lett. 81 (2002) 3568.
[19] B.D. Cullity, Elements of X-ray Diffraction, Addison-Wesley, Inc., London, 1978.
[20] B.E. Warren, X-ray Diffraction, Addison-Wesley, Reading, MA, 1969 (Chapter 12).
[21] A. Cebollada, D. Weller, J. Stichit, G.R. Harp, R.F.C. Farrow, R.F. Marks, R. Savoy, J.C. Scott, Phys. Rev. B 50 (1994) 3419.
[22] T. Shima, T. Moriguchi, S. Mitani, K. Takanashi, Appl. Phys. Lett. 80 (2002) 288.
[23] Y. Ding, S.A. Majetich, J. Kim, K. Barmak, H. Rollins, P. Sides, J. Magn. Magn. Mater. 284 (2004) 336.